Discovery and Development of ^{11}C-Lu AE92686 as a Radioligand for PET Imaging of Phosphodiesterase10A in the Brain

Jan Kehler[1], John Paul Kilburn[1], Sergio Estrada[2], Søren Rahn Christensen[3], Anders Wall[4], Alf Thibblin[2], Mark Lubberink[4], Christoffer Bundgaard[1], Lise Tøttrup Brennum[5], Björn Steiniger-Brach[5], Claus Tornby Christoffersen[6], Stine Timmermann[7], Mads Kreilgaard[8], Gunnar Antoni[2], Benny Bang-Andersen[1,8], and Jacob Nielsen[5]

[1]Division of Discovery Chemistry and DMPK, H. Lundbeck A/S, Valby, Denmark; [2]Preclinical PET Platform, Department of Medicinal Chemistry, Uppsala University, Uppsala, Sweden; [3]Department of Clinical Pharmacology, H. Lundbeck A/S, Valby, Denmark; [4]Nuclear Medicine and PET, Uppsala University and Uppsala University Hospital, Uppsala, Sweden; [5]Division of Synaptic Transmission, H. Lundbeck A/S, Valby, Denmark; [6]Department of Molecular Pharmacology, H. Lundbeck A/S, Valby, Denmark; [7]Department of Quantitative Pharmacology, H. Lundbeck A/S, Valby, Denmark; and [8]Department of Drug Design and Pharmacology, University of Copenhagen, Copenhagen, Denmark

Phosphodiesterase 10A (PDE10A) plays a key role in the regulation of brain striatal signaling, and several pharmaceutical companies currently investigate PDE10A inhibitors in clinical trials for various central nervous system diseases. A PDE10A PET ligand may provide evidence that a clinical drug candidate reaches and binds to the target. Here we describe the successful discovery and initial validation of the novel radiolabeled PDE10A ligand 5,8-dimethyl-2-[2-((1-^{11}C-methyl)-4-phenyl-1*H*-imidazol-2-yl)-ethyl]-[1,2,4]triazolo[1,5-*a*]pyridine (^{11}C-Lu AE92686) and its tritiated analog ^{3}H-Lu AE92686. **Methods:** Initial in vitro experiments suggested Lu AE92686 as a promising radioligand, and the corresponding tritiated and ^{11}C-labeled compounds were synthesized. ^{3}H-Lu AE92686 was evaluated as a ligand for in vivo occupancy studies in mice and rats, and ^{11}C-Lu AE92686 was evaluated as a PET tracer candidate in cynomolgus monkeys and in humans. **Results:** ^{11}C-Lu AE92686 displayed high specificity and selectivity for PDE10A-expressing regions in the brain of cynomolgus monkeys and humans. Similar results were found in rodents using ^{3}H-Lu AE92686. The binding of ^{11}C-Lu AE92686 and ^{3}H-Lu AE92686 to striatum was completely and dose-dependently blocked by the structurally different PDE10A inhibitor 2-[4-(1-methyl-4-pyridin-4-yl-1*H*-pyrazol-3-yl)-phenoxymethyl]-quinoline (MP-10) in rodents and in monkeys. In all species, specific binding of the radioligand was seen in the striatum but not in the cerebellum, supporting the use of the cerebellum as a reference region. The binding potentials (BP_{ND}) of ^{11}C-Lu AE92686 in the striatum of both cynomolgus monkeys and humans were evaluated by the simplified reference tissue model with the cerebellum as the reference tissue, and BP_{ND} was found to be high and reproducible—that is, BP_{ND}s were 6.5 ± 0.3 (n = 3) and 7.5 ± 1.0 (n = 12) in monkeys and humans, respectively. **Conclusion:** Rodent, monkey, and human tests of labeled Lu AE92686 suggest that ^{11}C-Lu AE92686 has great potential as a human PET tracer for the PDE10A enzyme.

Key Words: ^{11}C; ^{3}H; PET; PDE10A; brain imaging; Lu AE92686

J Nucl Med 2014; 55:1513–1518
DOI: 10.2967/jnumed.114.140178

Phosphodiesterase 10A (PDE10A) is predominantly expressed in medium spiny neurons and plays a key role in striatal signaling. During the past 10 y, large efforts have been made to develop PDE10A inhibitors for the treatment of schizophrenia (*1–3*). Preclinical evidence in several animal models suggests that PDE10A inhibitors can improve positive, negative, and cognitive symptoms of schizophrenia, and current clinical trials evaluate PDE10A inhibitors for the treatment of schizophrenia (*4*). Noninvasive imaging techniques such as PET may be useful for the clinical development of PDE10A inhibitors, because they may provide comparative data on the expression of the enzyme in healthy individuals and in individuals with brain disorders. Furthermore, a PDE10A PET ligand can be used to provide evidence that a clinical drug candidate reaches and binds to the target.

The PDE10A enzyme is likely to be a good PET target because of its high and selective expression in the striatum, which is phylogenetically conserved throughout mammalian species (*5*). Some attempts to visualize PDE10A by PET have recently been reported including the use of the moderately selective PDE10A inhibitor papaverine (*6*), an ^{18}F-labeled PQ-10 derivative (*7*), the clinical drug candidate MP-10 (*8*), and several ^{11}C- and ^{18}F-labeled analogs of 2-[4-(1-methyl-4-pyridin-4-yl-1*H*-pyrazol-3-yl)-phenoxymethyl]-quinoline (MP-10), including the ligand ^{18}F-JNJ41510417 (*9–11*). A first-in-human biodistribution and dosimetry study of the MP-10 derivative ^{18}F-JNJ-42259152 showed that this tracer displayed promising brain kinetics (*12*), and the potential of the ligand was supported by a test–retest study (*13*).

The aim of our study was to identify a new PET tracer for PDE10A. A 3-step strategy was pursued. First, candidate compounds were selected using the following in vitro and in vivo criteria: physical–chemical parameters within certain restrictions (*14*) (calculated 1-octanol-water partition coefficient at pH 7.4 [logD], between 1.5 and 3.5; calculated polar surface area, below, 0.70 nm^2 [70 Å^2]; molecular mass < 400 g/mol); high inhibitory activity against the human enzyme (half maximal inhibitory concentration

Received Mar. 19, 2014; revision accepted May 30, 2014.
For correspondence or reprints contact: Benny Bang-Andersen, H. Lundbeck A/S, Division of Discovery Chemistry and DMPK, Ottiliavej 9, DK-2500 Valby, Denmark.
E-mail: BAN@lundbeck.com
Published online Jul. 3, 2014.

< 10 nM); selectivity greater than 100-fold over other targets, for example, enzymes, receptors, and ion channels; high brain uptake (brain-to-plasma ratio, >0.4); and an easy radiolabeling in the last synthesis step. One such compound was 5,8-dimethyl-2-[2-([1-methyl]-4-phenyl-1*H*-imidazol-2-yl)-ethyl]-[1,2,4]triazolo[1,5-*a*]pyridine (Lu AE92686; logD, 3.0; calculated polar surface area, 0.49 nm^2 [49 $Å^2$]; molecular mass, 331; brain-to-plasma ratio [mice], 0.47; PDE10A half maximal inhibitory concentration, 0.39 nM; selectivity, >1,000-fold over PDE1b, PDE2, PDE3A, PDE4d6, PDE5a, PDE7b, PDE9, and PDE11 and >2,000-fold for the standard receptor and ion channel CEREP panel). The second step comprised synthesis of a tritiated version of Lu AE92686 (^{3}H-Lu AE92686, Fig. 1) and evaluation in rats and mice by an in vivo occupancy assay. Third, the ^{11}C-labeled ligand (^{11}C-Lu AE92686, Fig. 1) was synthesized and evaluated in PET studies in monkeys. This article reports the identification of ^{11}C-Lu AE92686 as a candidate for in vivo imaging of PDE10A and evaluation in humans.

MATERIALS AND METHODS

Chemistry

The synthesis of 2-[1,2-di-^{3}H-2-(1-methyl-4-phenyl-1*H*-imidazol-2-yl)-ethyl]-5,8-dimethyl-[1,2,4]triazolo[1,5-*a*]pyridine (^{3}H-Lu AE92686) was performed at Amersham (GE Healthcare) by treatment of trans-5,8-dimethyl-2-[(*E*)-2-(1-methyl-4-phenyl-1*H*-imidazol-2-yl)-vinyl]-[1,2,4]triazolo [1,5-*a*]pyridine (*15*) with tritium gas using palladium on carbon as catalyst. The radiochemical purity of ^{3}H-Lu AE92686 was above 90%, and the specific activity was 1.2 GBq/μmol.

The synthesis of 5,8-dimethyl-2-[2-([^{11}C-1-methyl]-4-phenyl-1*H*-imidazol-2-yl)-ethyl]-[1,2,4]triazolo-[1,5-*a*]pyridine was performed at Uppsala University by methylation of 5,8-dimethyl-2-[2-(4-phenyl-1*H*-imidazol-2-yl)-ethyl]-[1,2,4]triazolo[1,5-*a*]pyridine (*15*) with ^{11}C-methyliodide. ^{11}C-Lu AE92686 had radiochemical purity above 95% and specific radioactivity of about 40 GBq/μmol. A production batch generally resulted in 1.1 GBq of ^{11}C-Lu AE92686.

Ethical Issues

All animal experiments were approved by the local ethics committee for animal research and were performed in accordance with institutional as well as Danish and Swedish national rules and regulations.

The study was approved by the Swedish Medical Products Agency, the Regional Board of Medical Ethics, and the local radiation ethics committee at the Uppsala University Hospital. All subjects signed an informed consent form before inclusion.

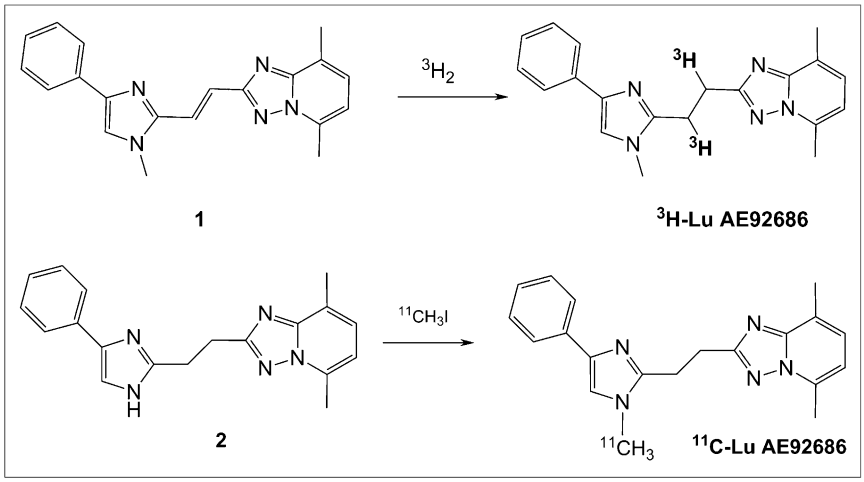

FIGURE 1. Synthesis of ^{3}H-Lu AE92686 and of ^{11}C-Lu AE92686.

In Vivo Studies in Rodents

In vivo binding studies were performed as described in the study by Larsen et al. (details in the supplemental data [available at http://jnm.snmjournals.org]) (*16,17*).

Dosimetry studies were performed in Sprague–Dawley rats injected in the tail vein with 8.1 ± 0.7 MBq of ^{11}C-Lu AE92686 in saline. One rat of each sex was sacrificed after 2, 5, 10, 20, and 40 min. Blood and 16 organs were immediately extracted, their radioactivity measured in a well counter, and the weight of the extracted tissues was determined. The organ radioactivity distribution from rats was extrapolated to humans, and residence times were calculated and used as an input for the OLINDA/EXM package (version 1.1; Vanderbilt University) (*18*) for estimation of organ equivalent and effective radiation doses.

In Vivo PET Binding Studies in Nonhuman Primates

PET Imaging. Two female cynomolgus monkeys (*Macaca fascicularis*) were used. Animals were sedated with ketamine (Ketalar [Pfizer]; 10 mg/kg) and maintained on a constant infusion of ketamine, 15 mg/kg/h, during transport. At arrival, they were intubated and maintained on sevoflurane (Sevofluran [Baxter]; concentration, 2%–5%) and artificial ventilation. Imaging was performed on a PET camera (SHR 7700 [Hamamatsu]; aperture, 30 cm; field of view, 12 cm; spatial resolution, 3.5 mm). The animal was placed on the camera bed (water-heated mat < 40°C) and covered to reduce loss of body temperature. Ringer-Acetate (Fresenius-Kabi; 0.5–1 mL/kg/h) was infused. Both monkeys first underwent a baseline scan. Then, 1 monkey received a second baseline scan during the same day, followed by a third scan starting 15 min after intravenous infusion of MP-10 (0.6 mg/kg) during 15 min. The second monkey underwent 2 more scans after infusion of MP-10 (0.11 and 1.5 mg/kg). All scans were performed with at least 2 h between injections to allow for decay of the radioactivity. The acquisition of PET data started simultaneously with intravenous bolus injection of 13 ± 2 MBq/kg of ^{11}C-Lu AE92686, followed by 1 mL of saline. Blood samples were taken at set times for measurement of whole-blood and plasma radioactivity concentrations, metabolite analysis, free fraction, and analysis of drug concentrations. Body temperature, heart rate, electrocardiogram, pCO_2, pO_2, SaO_2 (partial pressure of carbon dioxide, partial pressure of oxygen, and arterial oxygen saturation, respectively), and blood pressure were monitored throughout the PET study. Determination of free fraction in plasma was done by standard methods (supplemental data).

Image Reconstruction and Analysis. Attenuation correction was based on a transmission scan with a rotating ^{68}Ge rod source. The images were reconstructed by filtered backprojection with appropriate corrections and a 4-mm Hanning filter, resulting in a spatial resolution of about 4 mm. Image analysis was performed using VOIager software (GE Healthcare). Early (0–5 min) and late (40–90 min) summation images were created to visualize and delineate the regions of interest (ROIs) (striatum and cerebellum). Transaxial slices were used for drawing ROIs, and corresponding regions from both hemispheres were summed. After ensuring that no head movements had occurred during or in between scans, the striatum was manually delineated from late-summation baseline images and ROIs were imported to the other scans that had been obtained the same day. Early frames (0–5 min) were used for delineation of cerebellum. Decay-corrected time–activity curves were calculated for the ROIs and used in the kinetic modeling analysis. Modeling was performed using the simplified reference tissue

model (SRTM) (*19,20*). Values for the binding potential (BP_{ND}) in striatum were obtained and used to calculate the PDE10A inhibition in the drug-challenge experiments.

In Vivo PET Studies in Human Volunteers

Six healthy male subjects (mean age, 25.5 y; SD, 6.2) were included. As part of the screening procedure before the PET investigations, MR imaging scans were acquired to exclude subjects with clinically significant brain abnormalities and to provide anatomic images of the brain. Flair and T2 sequences were used for evaluation of possible brain abnormalities and T1 inversion recovery and a turbo field echo 3-dimensional sequence were conducted to enable coregistration of PET and MR imaging scans. MR imaging scans were obtained on a 1.5-T Achieva scanner (Philips Healthcare).

PET investigations were performed on an ECAT EXACT HR+ scanner (Siemens). After a 10-min transmission scan with rotating ^{68}Ge rods, approximately 370 MBq of ^{11}C-Lu AE92686 were administered intravenously as a bolus injection. Simultaneously, a dynamic emission scan was started in 3-dimensional mode, consisting of 25 time frames with progressive frame duration (6 × 10, 3 × 20, 2 × 30, 2 × 60, 2 × 150, 4 × 300, and 6 × 600 s) and a total duration of 90 min. Each subject underwent 2 scans during the same day with at least 2 h between injections for assessment of reproducibility. Images were reconstructed using normalization and attenuation-weighted ordered-subsets expectation maximization (6 iterations, 8 subsets), applying all appropriate corrections and a 4-mm Hanning filter, into an 128 × 128 matrix with a pixel size of 2 × 2 × 2.4 mm.

Blood Sampling. Continuous arterial blood sampling was done during the first 10 min of PET scanning, followed by discrete 5-mL arterial blood sampling at 5, 10, 15, 20, 45, and 60 min after tracer injection for measurement of whole-blood and plasma radioactivity concentrations and metabolite analysis to determine percentage intact ^{11}C-Lu AE92686 according to the method described above.

Data Analysis. Volumes of interest were drawn manually over the striatum and cerebellar cortex in summed PET images using VOIager and transferred to the dynamic dataset to obtain time–activity curves. Dynamic data were analyzed using single-tissue (2k) as well as irreversible (3k) and reversible (4k) 2-tissue-compartment models, including a fitted blood volume component, with nonlinear regression of the operational equations of these models to the measured striatal and cerebellar time–activity curves. The metabolite-corrected plasma time–activity curve was used as input curve. The optimal compartmental model was determined using the Akaike and Schwarz criteria (*21*). In addition, the Logan graphical method (*22*) was used to estimate the distribution volume (V_T). For all reversible models, the binding potential BP_{ND} was determined indirectly as the ratio of V_T in the striatum and cerebellum (V_T^{str} and V_T^{cer}, respectively) minus 1 (DVR-1). To evaluate the applicability of a reference tissue method, data were analyzed using SRTM and the reference Logan method (*23*). The robustness of each method was assessed using the test–retest scans, and reproducibility was calculated as the mean of the absolute differences between test and retest values divided by the average of test and retest.

RESULTS

Metabolite Analysis

In rats, plasma metabolism was fast, with about 15% of ^{11}C-Lu AE92686 remaining in plasma after 40 min. High-performance liquid chromatography analysis of plasma samples (Fig. 2A) revealed only metabolites with faster elution than ^{11}C-Lu AE92686, suggesting that mainly more hydrophilic metabolites were formed. High-performance liquid chromatography analysis of brain samples indicated only a small amount of metabolism in the brain or brain uptake of radioactive metabolites (data not shown).

In cynomolgus monkeys, ^{11}C-Lu AE92686 displayed rapid metabolism, with 65% ± 4%, 27% ± 4%, and 12% ± 2% intact tracer remaining in plasma at 5, 30 and 90, min after injection, respectively. In humans, the metabolism of ^{11}C-Lu AE92686 was considerably slower than in monkeys, and the rate of metabolism was similar for all 6 subjects. The percentage of intact ^{11}C-Lu AE92686 in human plasma is shown in Figure 2B. One hour after tracer administration, about 70% of the radioactivity measured was still originating from the tracer itself whereas 30% was related to radiolabeled metabolites.

In Vivo Studies in Rodents

In rats as well as in mice, ^{3}H-Lu AE92686 showed high total binding levels in the striatum and low levels in the cerebellum (Fig. 3), which is in agreement with the PDE10A expression pattern. We therefore selected the cerebellum as a reference region defining the level of nonspecific binding of the tracer. In an initial experiment, 3 doses of ^{3}H-Lu AE92686 (107.3, 214.6, or 307.1 kBq) were injected in mice, and high specific binding was observed in the striatum, compared with cerebellum, demonstrating a high signal-to-noise (S/N) ratio at all 3 doses (S/N > 50; Fig. 3A). A similar high S/N ratio was observed at doses of 240.5 and 455.1 kBq in rats (S/N > 50; Fig. 3B). The timing of radioligand dosing was varied from 5 to 20 min before measurement, and with all treatment times a more than 50-fold S/N ratio was obtained (Fig. 3C). Guided by these data, a dose of 92.5 kBq of ^{3}H-Lu AE92686 for mice and a dose of 222 kBq for rats were selected for in vivo binding experiments. The selective PDE10A inhibitor MP-10, which is structurally unrelated to Lu AE92686, was tested for its ability to block ^{3}H-Lu AE92686 binding in the striatum. MP-10 blocked ^{3}H-Lu AE92686 binding to rat striatum in a dose-dependent manner, with a median effective dose of 1.2 mg/kg (Fig. 3D). MP-10 blocked ^{3}H-Lu AE92686 binding in the striatum but not the cerebellum, validating the use of the cerebellum as a reference region (data not shown).

On the basis of the dosimetry studies in rats, the effective dose in humans is estimated as 3.1 μSv/MBq, corresponding to 1.1 mSv for a typical administration of 370 MBq (data not shown). Data acquired from toxicologic studies permitted the administration of ^{11}C-Lu AE92686 to human subjects (H. Lundbeck A/S, unpublished data, 2012).

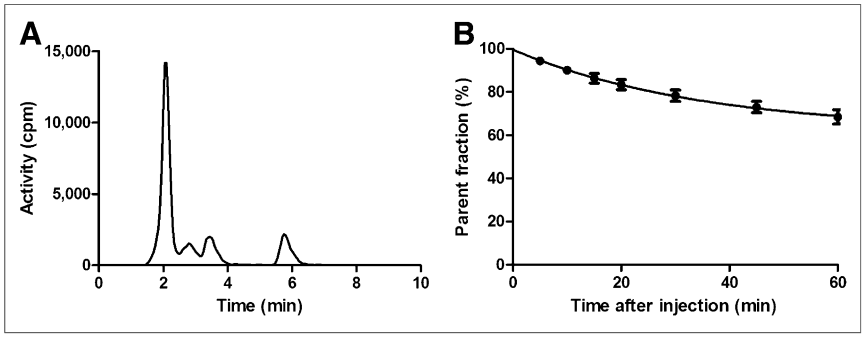

FIGURE 2. (A) High-performance liquid chromatography radio detector analysis of plasma from rat removed 40 min after injection of ^{11}C-Lu AE92686. Peak farthest to the right is intact tracer. (B) Percentage of intact ^{11}C-Lu AE92686 in plasma in humans (6 subjects, 12 scans), mean ± SD.

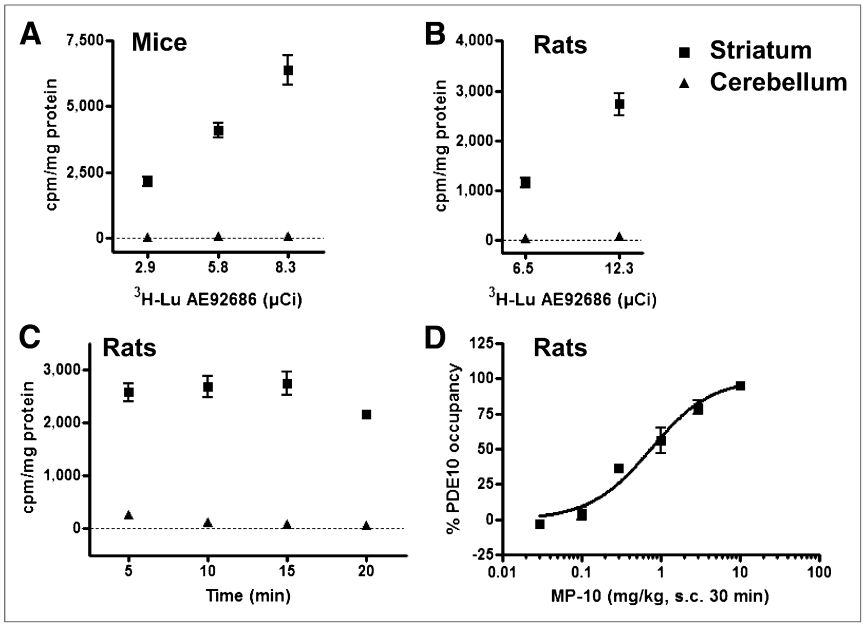

FIGURE 3. (A) ^{3}H-Lu AE92686 total binding levels in striatum and in cerebellum of mice 10 min after dosing (n = 5/group). (B) ^{3}H-Lu AE92686 total binding levels in striatum and in cerebellum of rats 15 min after dosing (n = 6/group). (C) PDE10A binding of ^{3}H-Lu AE92686 in rats as function of time elapsed after injection of tracer (n = 6/group). (D) Inhibition of ^{3}H-Lu AE92686 binding in rat striatum by varying doses of MP-10 administered subcutaneously 30 min before measurement (n = 6/group). All data presented as mean ± SEM.

In Vivo PET Binding Studies in Nonhuman Primates

The specific activity of ^{11}C-Lu AE92686 was 135 ± 30 GBq/μmol (n = 6). The free fraction of ^{11}C-Lu AE92686 in the plasma of the cynomolgus monkeys was 3.9% ± 1%, and MP-10 administration did not affect the distribution between free and bound tracer in plasma (data not shown). PET imaging revealed selective uptake of ^{11}C-Lu AE92686 in the striatum of the monkeys (Fig. 4) consistent with PDE10A expression. Analysis of the time–activity curves (Fig. 5) showed that ^{11}C-Lu AE92686 entered the brain rapidly and accumulated in the striatum. It reached a maximum after 15–20 min and then gradually decreased. In the cerebellum, rapid washout was observed. BP_{ND} for the striatum was calculated using the SRTM with the cerebellum as a reference region. The resulting BP_{ND} in baseline studies was 6.5 ± 0.3 (4%) and showed little variance. The test–retest PET scans displayed lower variance—that is, BP_{ND} was 6.6 ± 0.2 (2%). Plasma concentrations after 3 different doses of MP-10 are depicted graphically in Figure 5A. MP-10 dose-dependently blocked ^{11}C-Lu AE92686 uptake in the striatum but not in the cerebellum, confirming the specificity of striatal uptake and the use of the cerebellum as a reference region (Fig. 5D). The dose-dependent decrease in striatal ^{11}C-Lu AE92686 BP_{ND} could be fitted to a 1-site model (Fig. 5B).

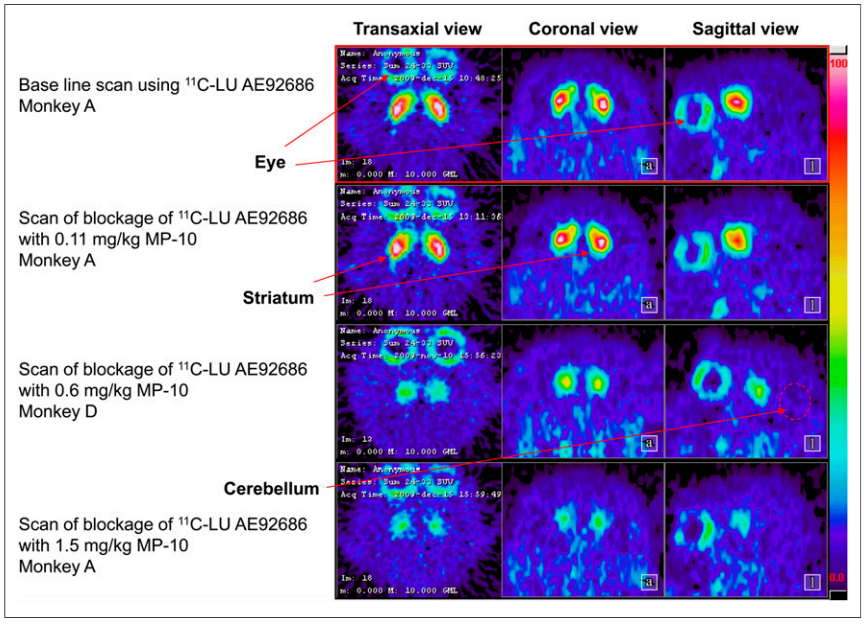

FIGURE 4. Standardized uptake value (SUV) images (15–90 min) at baseline and after blocking studies with ^{11}C-Lu AE92686 in the 2 monkeys. Pseudocolor scale is shown on outmost right, and 0%–100% spans from SUV 0 to 10. Sections displayed visualize the striatum, which is clearly observed.

In Vivo PET Studies in Human Volunteers

The specific activity of ^{11}C-Lu AE92686 used for human studies was 37 ± 18 GBq/μmol. Injected doses varied between 249 and 478 MBq, with an average of 423 MBq (scan 1) and 464 MBq (scan 2). The uptake of ^{11}C-Lu AE92686 in the human brain is illustrated with standardized uptake value PET images from a typical subject (Fig. 6). As in the monkeys, ^{11}C-Lu AE92686 uptake was clearly strongest in the striatum, where PDE10A is predominantly expressed (*5*).

Average time–activity curves of the 6 subjects for the test and retest scans for the striatum and cerebellum are shown in Figure 7. ^{11}C-Lu AE92686 exhibited selective uptake in the striatum. The uptake in the striatum increased gradually with time, peaking 40 min after injection, and thereafter slowly decreased. The cerebellum showed a low apparent uptake, which reached the maximum level during the first minute after tracer administration.

The applicability of single-tissue (2k) as well as irreversible (3k) and reversible (4k) 2-tissue-compartment models was assessed. In the striatum, the 2k, 3k, and 4k models were preferred in 6, 1, and 5 of 12 cases, respectively, according to the Akaike criterion, and in 7, 3, and 2 cases according to the Schwarz criterion. In the cerebellum, these numbers were 1, 11, and 0 and 3, 9, and 0, respectively. On the basis of these results, the 3k model was discarded for further analysis of striatal data. The reproducibility and absolute and relative repeatability of BP_{ND} and DVR-1 in the striatum are given in Table 1.

The cerebellar time–activity curves could not be fitted robustly by any of the plasma-input compartment models. The 2k model

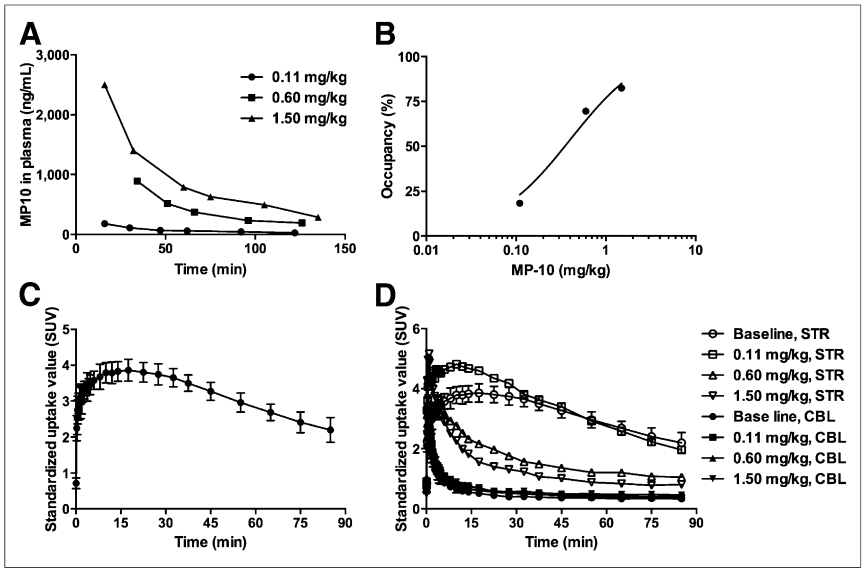

FIGURE 5. Study in cynomolgus monkeys. (A) Plasma concentration of MP-10 at different time points after administration. (B) Blocking (percentage occupancy) of ^{11}C-Lu AE92686 binding in striatum (STR) plotted against 3 doses of MP-10. Line shows nonlinear fit of simple competition curve to data. (C) Average striatal time–activity curves from 3 baseline studies. Error bars represent SD. (D) Time–activity curves of ^{11}C-Lu AE92686 in striatum and cerebellum (CBL) in studies with tracer alone (baseline) and after challenge with 3 doses of MP-10.

did not provide accurate fits, whereas the parameters in the 3k and 4k models had large standard errors, resulting in a large uncertainty in V_T^{cer} and, correspondingly, in BP_{ND} in plasma-input compartment models as seen in Table 1. DVR-1 as determined using the Logan method with plasma input was consequently used for validation of both reference tissue methods (a graphical plot is shown in the supplemental data). Both reference methods correlated well with DVR-1 as based on plasma-input Logan (R^2 = 0.98 for both). Therefore, both SRTM and reference Logan analysis with the cerebellum as a reference region can be considered robust models to assess the BP_{ND} of ^{11}C-Lu AE92686, and the estimates of striatal BP_{ND} using SRTM for all scans showed little variation, with a mean striatal BP_{ND} of 7.5 ± 1.0 (n = 12 scans).

DISCUSSION

The aim of this study was to develop a PET ligand for in vivo imaging of the PDE10A enzyme in the brain and evaluation of target engagement of PDE10A ligands. Lu AE92686 was selected as the most promising candidate from an extensive research program. The compound was radiolabeled with tritium and evaluated in vivo in rodents. There was a significant accumulation of the tracer in the striatum but not in the cerebellum in accordance with the reported distribution of PDE10A, and ^{3}H-Lu AE92686 was an excellent in vivo binding ligand for robust and good throughput determination of in vivo occupancy of PDE10 ligands in mice and rats. The S/N ratio for ^{3}H-Lu AE92686 in in vivo binding (striatum vs. cerebellum) was high (S/N > 50) as compared with in vivo binding with tritiated versions of established PET ligands such as the serotonin transporter ligand MADAM (S/N = 4, data not shown) and the dopamine D_2 receptor ligand raclopride (S/N = 20, data not shown), encouraging us to proceed with ^{11}C labeling of Lu AE92686, which was evaluated in vivo in cynomolgus monkeys and in humans. The PET data could be analyzed using the SRTM with the cerebellum as a reference tissue. ^{11}C-Lu AE92686 displayed high BP_{ND} and selectivity for the striatum in both cynomolgus monkeys (BP_{ND}, 6.5 ± 0.26 [n = 3]) and humans (BP_{ND}, 7.5 ± 1.0 [n = 12]), and only the striatum had measurable uptake of the tracer in the PET scans. The brain kinetics of ^{11}C-Lu AE92686 indicated that the cerebellum could be used as a reference region, consistent with the negligible PDE10A expression in the cerebellum.

Moreover, the binding of ^{11}C-Lu AE92686 to striatum in cynomolgus monkeys was dose-dependently blocked by the structurally different PDE10A inhibitor MP-10. A dose-dependent decrease in BP_{ND} of ^{11}C-Lu AE92686 was observed after challenge with MP-10 in the cynomolgus monkeys using 3 doses of MP-10 as the blocking compound (0.11, 0.6, and 1.5 mg/kg), which resulted in 18%, 70%, and 82% occupancy of PDE10A, respectively.

Plasma clearance in rats and monkeys was fast, whereas the clearance was considerably slower in humans. Radiolabeled metabolites from ^{11}C-Lu AE92686 were assessed in rat plasma without signs of lipophilic metabolites.

The evaluation of the ligand in healthy human volunteers revealed an excellent test–retest variability and low variability between subjects.

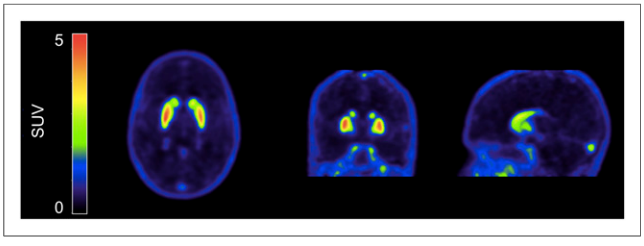

FIGURE 6. ^{11}C-Lu AE92686 uptake in human brain (sum image 15–90 min after injection).

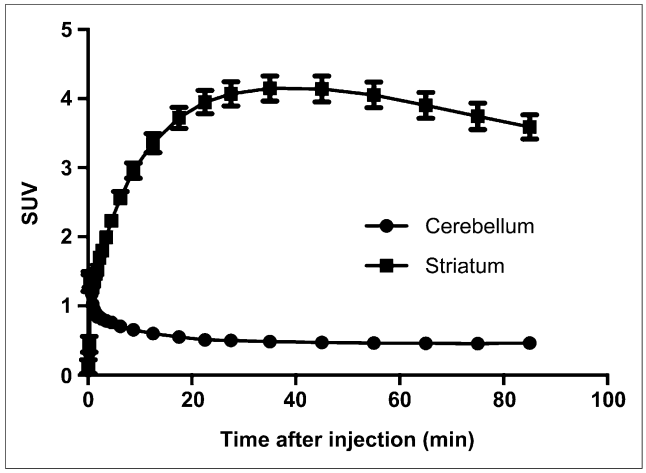

FIGURE 7. Average time–activity curves for all subjects (6 subjects, each scanned twice, mean ± SD), showing standardized uptake values (SUVs) of ^{11}C-Lu AE92686 over time in striatum and cerebellum. In cerebellum, error bars were of size comparable to symbols and were omitted.

TABLE 1
Reproducibility and Repeatability of BP_{ND} and DVR-1 Calculated by Different Compartmental Models

Model	Reproducibility (%)	Repeatability (%)	Repeatability (absolute)
2k*	10	35	7.7
4k*	90	218	10.2
Logan*	7	22	1.3
SRTM	6	20	1.2
Reference Logan	6	19	1.2

*BP_{ND} calculated indirectly as $V_T^{str}/V_T^{cer} - 1$.

Single-tissue as well as irreversible and reversible 2-tissue-compartment models were evaluated using a test–retest protocol. The single-tissue-compartment model gave the best fits in the striatum according to the Akaike and Schwartz criteria, meaning that specific binding cannot be distinguished from free tracer in tissue and nonspecific binding and that direct estimation of BP_{ND} in the striatum is not possible. In the cerebellum, the irreversible 2-tissue-compartment model was preferred over the single-tissue-compartment model. This second compartment, albeit small, may either represent nonspecific binding of the tracer or may be a spurious compartment caused by brain uptake of radioactive metabolites. Metabolite uptake would be expected to be uniform throughout the brain, but a second compartment cannot be detected in the striatum, possibly because it is negligible, compared with the specific striatal signal. A small amount of uniform uptake of radioactive metabolites in the brain is not likely to significantly affect indirect BP_{ND} estimates using a reference region (*24*). Plasma-input Logan analysis provided robust estimates of V_T^{cer} and V_T^{str} and could be used to indirectly estimate BP_{ND}. The use of SRTM and reference Logan analysis was thus validated by comparison with BP_{ND} values as based on plasma-input Logan analysis. Because a high correlation ($R^2 = 0.98$) was found between BP_{ND} estimated by SRTM and reference Logan analysis, both SRTM and reference Logan analysis with the cerebellum as a reference region were robust models to assess BP_{ND} of ^{11}C-Lu AE92686 in the human brain.

CONCLUSION

Our results suggest that ^{11}C-Lu AE92686 has great potential as a human PET tracer for evaluation of basal PDE10A levels and occupancy of compounds targeting this enzyme in monkeys and humans. Furthermore, ^{3}H-Lu AE92686 was an excellent tool for assessing in vivo occupancy of PDE10 ligands in mice and rats, allowing translational studies to be performed. SRTM was shown to be an appropriate kinetic model, allowing a simple study setup in future PET studies. Thus, ^{11}C-Lu AE92686 has potential for assessing whether PDE10A competitive inhibitors display target engagement in humans within the expected therapeutic window and thus facilitates future clinical trials investigating novel PDE10A inhibitors.

DISCLOSURE

The costs of publication of this article were defrayed in part by the payment of page charges. Therefore, and solely to indicate this fact, this article is hereby marked "advertisement" in accordance with 18 USC section 1734. No potential conflict of interest relevant to this article was reported.

ACKNOWLEDGMENTS

We thank Mimmi Lidholm, Annie Bjurebäck, Maj Wiberg, Marie Åhman, Lars Lindsjö, Margaretha Sprycha, Helena Wilking, and Veronica Asplund for their assistance in the clinical and preclinical PET studies.

REFERENCES

1. Menniti FS, Chappie TA, Humphrey JM, et al. Phosphodiesterase 10A inhibitors: a novel approach to the treatment of the symptoms of schizophrenia. *Curr Opin Investig Drugs.* 2007;8:54–59.
2. Chappie T, Humphrey J, Menniti F, et al. PDE10A inhibitors: an assessment of the current CNS drug discovery landscape. *Curr Opin Drug Discov Devel.* 2009;12:458–467.
3. Kehler J, Kilburn JP. Patented PDE10A inhibitors: novel compounds since 2007. *Expert Opin Ther Pat.* 2009;19:1715–1725.
4. Kehler J, Nielsen J. PDE10A inhibitors: novel therapeutic drugs for schizophrenia. *Curr Pharm Des.* 2011;17:137–150.
5. Coskran TM, Morton D, Menniti FS, et al. Immunohistochemical localization of phosphodiesterase 10A in multiple mammalian species. *J Histochem Cytochem.* 2006;54:1205–1213.
6. Tu Z, Xu J, Jones LA, Li S, Mach RH. Carbon-11 labeled papaverine as a PET tracer for imaging PDE10A: radiosynthesis, in vitro and in vivo evaluation. *Nucl Med Biol.* 2010;37:509–516.
7. Funke U, Deuther-Conrad W, Schwan G, et al. Radiosynthesis and radiotracer properties of a7-(2-[^{18}F]fluoroethoxy)-6-methoxypyrrolidinylquinazoline for imaging of phosphodiesterase 10A with PET. *Pharmaceuticals (Basel).* 2012;5:169–188.
8. Tu Z, Fan J, Li S, et al. Radiosynthesis and in vivo evaluation of [^{11}C]MP-10 as a PET probe for imaging PDE10A in rodent and non-human primate brain. *Bioorg Med Chem.* 2011;19:1666–1673.
9. Celen S, Koole M, De AM, et al. Preclinical evaluation of ^{18}F-JNJ41510417 as a radioligand for PET imaging of phosphodiesterase-10A in the brain. *J Nucl Med.* 2010;51:1584–1591.
10. Andrés J-I, Angelis MD, Alcázar J, et al. Synthesis, in vivo occupancy, and radiolabeling of potent phosphodiesterase subtype-10 inhibitors as candidates for positron emission tomography imaging. *J Med Chem.* 2011;54:5820–5835.
11. Andres-Gil JI, Bormans GMR, De Angelis M, Celen S, inventors; Janssen Pharmaceutica N, assignee. Radiolabelled PDE10 ligands. WO2010097367. 2010.
12. Van Laere K, Ahmad RU, Hudyana H, et al. Human biodistribution and dosimetry of ^{18}F-JNJ42259152, a radioligand for phosphodiesterase 10A imaging. *Eur J Nucl Med Mol Imaging.* 2013;40:254–261.
13. Van Laere K, Ahmad RU, Hudyana H, et al. Quantification of ^{18}F-JNJ-42259152, a novel phosphodiesterase 10A PET tracer: kinetic modeling and test-retest study in human brain. *J Nucl Med.* 2013;54:1285–1293.
14. Zhang L, Villalobos A, Beck EM, et al. Design and selection parameters to accelerate the discovery of novel central nervous system positron emission tomography (PET) ligands and their application in the development of a novel phosphodiesterase 2A PET ligand. *J Med Chem.* 2013;56:4568–4579.
15. Ritzen A, Kehler J, Langgaard M, et al., inventors; Lundbeck A/S, assignee. Novel phenylimidazole derivatives as PDE10A enzyme inhibitors for treating neurodegenerative disorder, psychiatric disorder, or drug addiction. WO2009152825. 2009.
16. Larsen AK, Brennum LT, Egebjerg J, et al. Selectivity of ^{3}H-MADAM binding to 5-hydroxytryptamine transporters in vitro and in vivo in mice; correlation with behavioural effects. *Br J Pharmacol.* 2004;141:1015–1023.
17. Smith PK, Goeke NM, Olson BJ, Klenk DC. Measurement of protein using bicinchoninic acid. *Anal Biochem.* 1985;150:76–85.
18. Stabin MG, Sparks RB, Crowe E. OLINDA/EXM: the second-generation personal computer software for internal dose assessment in nuclear medicine. *J Nucl Med.* 2005;46:1023–1027.
19. Lammertsma AA, Hume SP. Simplified reference tissue model for PET receptor studies. *Neuroimage.* 1996;4:153–158.
20. Lammertsma AA, Bench CJ, Price GW, et al. Measurement of cerebral monoamineoxidase B activity using L-[^{11}C]deprenyl and dynamic positron emission tomography. *J Cereb Blood Flow Metab.* 1991;11:545–556.
21. Akaike H. A new look at the statistical model identification. *IEEE Trans Automat Contr.* 1974;19:716–723.
22. Logan J, Fowler JS, Volkow ND, et al. Graphical analysis of reversible radioligand binding from time-activity measurements applied to [N-11 C-methyl]-(-)-cocaine PET studies in human subjects. *J Cereb Blood Flow Metab.* 1990;10:740–747.
23. Logan J, Fowler JS, Volkow ND, et al. Distribution volume ratios without blood sampling from graphical analysis of PET data. *J Cereb Blood Flow Metab.* 1996;16:834–840.
24. Yaqub M, Boellaard R, van Berckel BN, et al. Evaluation of tracer kinetic models for analysis of [^{18}F]FDDNP studies. *Mol Imaging Biol.* 2009;11:322–333.

JNM The Journal of NUCLEAR MEDICINE

Discovery and Development of ^{11}C-Lu AE92686 as a Radioligand for PET Imaging of Phosphodiesterase10A in the Brain

Jan Kehler, John Paul Kilburn, Sergio Estrada, Søren Rahn Christensen, Anders Wall, Alf Thibblin, Mark Lubberink, Christoffer Bundgaard, Lise Tøttrup Brennum, Björn Steiniger-Brach, Claus Tornby Christoffersen, Stine Timmermann, Mads Kreilgaard, Gunnar Antoni, Benny Bang-Andersen and Jacob Nielsen

J Nucl Med. 2014;55:1513-1518.
Published online: July 3, 2014.
Doi: 10.2967/jnumed.114.140178

The Journal of Nuclear Medicine is published monthly.
SNMMI | Society of Nuclear Medicine and Molecular Imaging
1850 Samuel Morse Drive, Reston, VA 20190.
(Print ISSN: 0161-5505, Online ISSN: 2159-662X)

SNMMI SOCIETY OF NUCLEAR MEDICINE AND MOLECULAR IMAGING